Hindawi
Advances in Tribology
Volume 2023, Article ID 9917497, 11 pages
https://doi.org/10.1155/2023/9917497

Research Article

Investigation on the Cutting Force and Surface Quality in Harmonically Vibrated Broaching (HVB)

Amirreza Mohammadian[1] and Mahdi Sadeqi Bajestani[2]

[1]*Mechanical Engineering Department, Sadjad University, Mashhad, Iran*
[2]*Mechanical Engineering Department, Ferdowsi University of Mashhad, Mashhad, Iran*

Correspondence should be addressed to Mahdi Sadeqi Bajestani; msadeqib@gmail.com

Received 1 February 2023; Revised 15 April 2023; Accepted 29 April 2023; Published 25 May 2023

Academic Editor: Lijesh Koottaparambil

This paper investigates the broaching process of phosphor-bronze (C54400) under different cutting conditions, and the influential factors on cutting force and surface quality are studied. The simulated cutting force implementing the force model based on the energy components also agrees with the results of experiments. In the first part, different cutting velocities of $V_C = 5$, 10, 15, and 20 m/min are studied. In the second part, harmonic vibrations in the form of a sine wave with precise amplitude ($A = 1$ m/min) and frequencies ($F = 55$, 65, 85, and 95 Hz) are added in the direction of the cutting velocity. The results revealed that an increase in the cutting velocity from 5 to 20 m/min results in a 40% enhancement in surface quality and a 20% decrease in the cutting force. Additionally, harmonic vibrations of higher frequencies can also contribute to a 35% higher surface quality and a 20% lower cutting force. This study will ultimately improve productivity in industries where broaching is considered the main manufacturing approach, such as automotive and aerospace, in which precision and accuracy are of paramount importance.

1. Introduction

Broaching is one of the cutting processes, similar to sawing, which allows the production of different shapes on the machined surface, e.g., flat, grooved, or even formed surfaces. It is a single-path operation and is commonly carried out as a postturning/postmilling process. Broaching is economical, particularly in mass production, and can produce surfaces with the desired roughness and high geometrical accuracy [1].

Broaching is commonly used in high-tech industries such as automotive and aerospace, where precision and accuracy are important [2]. It is a process in which complex shapes can be produced with a high surface finish, where the use of lubrication is common [3, 4]. The broaching tool typically consists of three sections: roughing, finishing, and calibration. "Rise per tooth" is the parameter by which the material removal rate is decided. Other influential geometrical features include depth of cut (f_z), rake angle (γ), clearance angle (α), and width of the land (b_{fa}), which may differ depending on the section of the tool [5] (roughing, finishing, or calibration) and mechanical properties of the workpiece material (Figure 1).

One problem with the broaching process is tool wear, which mostly affects edge flank surfaces (flank wear). However, it can also manifest as crater wear on the rake face. Multiple wear reasons can take place at once. However, abrasion is the most typical. A small degree of plastic deformation can also be seen at the tips of the teeth. Additionally, unexpected vibrations may cause edge chipping. Other processes that depend more on temperature are uncommon since coolant oils regulate process temperature [7].

Forst [8] experimentally defined broaching and investigated the effective causes and parameters of the process in detail. Although it was published in 1932, it has never been considered outdated. Terry and Cutright [9] introduced a CAD (computer-aided design) process for determining both the optimal values and operating conditions for the broaching process. Kishawy et al. [10]

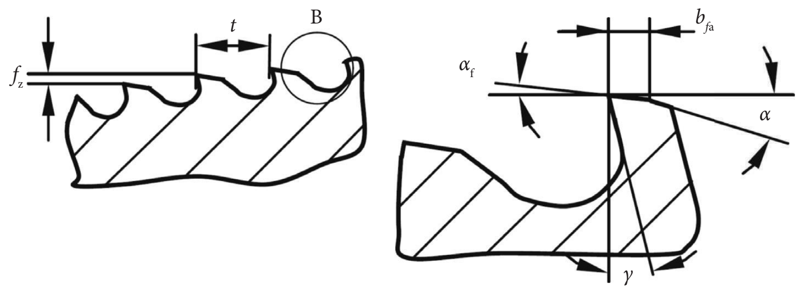

FIGURE 1: Geometrical features of the broaching tool [6].

surveyed the mechanics of cutting and the effects of broaching tool teeth on the surface roughness of the workpiece material through an energy-based analysis, and Teti et al. [11] reviewed the monitoring of machining operation approaches and signal-processing strategies as well as their industrial applications.

Hosseini and Kishawy [12] presented a force model for predicting cutting forces and chip load in orthogonal and oblique broaching processes by introducing the cutting edge as a parametric B-spline curve. Axinte et al. [13] studied the relationship between the quality of the machined surface and the output signals of cutting force, vibration, and acoustics sensors. They implemented surface roughness and optical and scanning electron microscopy to evaluate surface quality parameters such as profile deviation, chatter marks, and burr formation. Özelkan et al. [14] studied a methodology to design a broaching tool, considering geometrical and physical limitations optimally. Complementary research was carried out by Ozturk and Budak [15], where they studied a broaching tool optimization method implementing cutting models and finite element analysis (FEA) and abridged the outcome of the research into analytical forms that can be used in industrial applications. Axinte and Gindy [16] monitored the tool condition in different broaching conditions using the output signals extracted from some sensors in different tool conditions. They concluded that acoustic emission, vibration, and cutting force sensors are sensitive to broaching tool conditions.

Meng et al. [17] did thorough research on modelling and analysis of the broaching process enhanced by a forced vibration on cutting velocity created by a single harmonic motion. They also considered three important notes: the cutting force of a single tooth, the number of teeth engaged, and the influence of simple harmonic motion. Then, they presented two single-tooth and two multiteeth models for broaching based on the empirical approach and shear angle theory. Finally, they verified the results with experimental tests.

In a recent study, Orouji et al. [18] studied the influence of cutting velocity on surface quality in the broaching process on the workpiece material of Al-7075, resulting in observations of enhanced surface quality and reduced cutting force with the increase of cutting velocity. Later, Bajestani et al. [19] studied the effect of vibrations in cutting velocity on the cutting force and surface roughness in Al7075-T6 broaching. They concluded that increasing cutting velocity will lead to lower cutting force and increased surface quality.

In this paper, we propose the concept of harmonically vibrated broaching (HVB) with different frequencies to reduce the cutting force and improve the surface roughness of the process. We implemented the numerical force model using the energy balance and performed the experiment with phosphor-bronze (C54400) material to verify the results.

2. Force Model Using Energy Balance

According to the model proposed by Kishawy et al. [10], the cutting force can be quantified as a function of power components as

$$\begin{aligned} F_C &= \frac{P_C}{V_C} \\ &= \frac{P_{fF} + P_{fR} + P_{ch} + P_{mn-ce} + P_{pd}}{V_C}, \end{aligned} \tag{1}$$

where P_C (N.m/min) is the power consumed for the cutting process, P_{fF} and P_{fR} are the power consumption at the tool-workpiece and tool-chip interface, respectively, P_{pd} is the consumed power for the plastic deformation of the workpiece for material removal, P_{ch} is the power used for the formation of the new surface, and $P_{mn\text{-}ce}$ is the power consumed due to the combined influence of the minor cutting edge, and V_C (m/min) is the cutting velocity.

2.1. Tool Workpiece Interface. The consumed power due to friction between the workpiece and the tool is calculated as [20]

$$P_{fF} = F_{fF} V, \tag{2}$$

where V (m/min) is the chip velocity and F_{fF} is the friction force between the tool and workpiece, which can be calculated through.

$$F_{fF} = 0.625 \tau_y \rho_{ce} l_{ac} \sqrt{\frac{Br}{\sin \alpha_{nw}}}, \tag{3}$$

where Br is the Briks similarity criterion:

$$Br = \frac{\cos\gamma}{\xi - \sin\gamma}, \tag{4}$$

and γ (deg) is the normal rake angle, ξ is the chip comparison ratio, τ_y (N/m^2) is the shear strength of the workpiece material, ρ_{ce} (m) is the radius of the cutting edge, α_{nw} (deg) is the normal flank angle, and l_{ac} (m) is the engaged length of the edge in the cutting process. The chip comparison ratio, ξ, is calculated as

$$\xi = \frac{t_{2T}}{t_{1T}}, \tag{5}$$

where t_{1T} (m) is the uncut chip thickness and t_{2T} (m) is the formed chip thickness.

Substituting (3)–(5) in (2) results in

$$P_{fF} = 0.625\tau_y\rho_{ce}l_{ac}V\sqrt{\frac{\cos\gamma}{(\sin\alpha_{nw})(t_{2T} - t_{1T}\sin\gamma)}}. \tag{6}$$

2.2. Tool-Chip Interface. The power consumed at the tool-chip interface originating from the friction between tool and chip on the rake face P_{fR} is calculated as

$$P_{fR} = \tau_c l_c b_{1T}\frac{V_C}{\xi}, \tag{7}$$

where $\tau_c = 0.28\,\sigma_R$ (N/m^2) is the average shear stress at the tool-chip contact zone, σ_R (N/m^2) is the ultimate tensile strength of the workpiece material, b_{1T} (m) is the chip width, and l_c (m) is tool-chip contact length and is calculated as

$$l_c = t_{1T}\xi^k, \tag{8}$$

where $k = 1.5$ when $\xi < 4$ and $k = 1.3$ for $\xi \geq 4$. In this research, experiments show that chip compression ratio is approximately 5, which will be discussed in the following sections. Substituting (5) and (8) in (7), we will have

$$P_{fR} = 0.28\sigma_R t_{1T}^{0.7} t_{2T}^{0.3} b_{1T} V_C. \tag{9}$$

2.3. Formation of New Surfaces and the Effect of Minor Cutting Edge. The power consumed for the formation of new surfaces is calculated as

$$P_{ch} = E_{fr} f_{cf}, \tag{10}$$

where f_{cf} is the frequency of chip formation and E_{fr} is the energy of fracture. P_{ch} is negligible in the broaching process due to the low cutting velocity and, consequently, the low frequency of chip formation [10]. Based on the numerical calculations considering the low cutting velocities employed in this study (5, 10, and 15 m/min), this parameter is in a scale of 10^{-5}, which can be neglected compared to other power elements. Besides, as far as broaching does not have a minor cutting edge, the parameter $P_{mn\text{-}ce}$ is equal to zero [10].

2.4. Plastic Deformation. The layer being removed from the workpiece consumes power calculated as [20]

$$p_{pd} = \frac{V_C A_\omega K\left(\ln t_{2T}^{1.5} - \ln t_{1T}^{1.5}\right)^{n+1}}{n+1}, \tag{11}$$

where K (N/m^2) is the strength coefficient, n is the hardening exponent of the workpiece material, and A_ω (m^2) is the uncut chip cross-sectional area. Substituting(6), (9), and (11) in (1) results in a straightforward equation for measuring cutting force per tooth in the broaching process ((12)).

$$F_C = \frac{0.625\tau_y\rho_{ce}l_{ac}V}{V_C} \times \sqrt{\frac{\cos\gamma}{(\sin\alpha_{nw})(t_{2T} - t_{1T}\sin\gamma)}} + 0.28\sigma_R t_{1T}^{0.7} t_{2T}^{0.3} b_{1T} + \frac{A_\omega K\left(\ln t_{2T}^{1.5} - \ln t_{1T}^{1.5}\right)^{n+1}}{n+1}. \tag{12}$$

The cutting force for a single tooth in the broaching process is calculated using (12). To determine the total cutting force, it has to be multiplied by the number of teeth simultaneously engaged in the workpiece.

In the simulations, broaching is assumed as a plain strain process; therefore, the chip width before and after cutting is considered equal. Consequently, b_{T1} would be the length of the cutting edge ($l_{ac} = b_{T1}$), and the true uncut chip thickness, t_{1T}, is also considered to be equal to rise per tooth ($t_{1T} = f_z$).

Consequently, as illustrated in (5), where ξ is defined as the ratio of the formed chip thickness and uncut chip thickness, dividing the measured thickness of the formed chip resulting from the experimental broaching process, shown in Table 1, by the value of already known uncut chip thickness, the mean value of chip compression ratio is determined.

Other required parameters to determine the cutting force using (12) are related to the geometrical features of the broaching tool and mechanical properties of the workpiece material, which will be discussed in the following section.

3. Experimental Setup

The experimental setup for verifying the force model using energy balance consists of the broaching tool, hydraulic cylinder, valves, accumulators, load cell, linear scale, and fixture, which will be discussed in detail in the following sections. The overall specifications of the servohydraulic system are tabulated in Table 2.

In Figure 2, the position and arrangement of each component of the experimental setup and the direction of the broaching process are shown.

Figure 3 also demonstrates the hydraulic circuit of the experimental setup.

The tool implemented for this research is designed and manufactured for these specific setup configurations and research series. The RENISHAW cyclone digitizer, with an accuracy of 1 μm, is utilized to extract accurate geometrical features of the broaching tool. The broaching tool specifications are mentioned in Table 3.

Table 1: Formed and uncut chip thickness for different cutting velocities.

V_C	t_{1T}	t_{2T}	ξ
5	0.09	0.45	5.00
10	0.09	0.45	5.00
15	0.09	0.46	5.11
20	0.09	0.46	5.11

Table 2: Hydraulic system specifications.

Working temperature	40–45°C
Working pressure	150 bar
Maximum speed	30 m/min
Maximum pressure	350 bar
Working stroke	300 mm

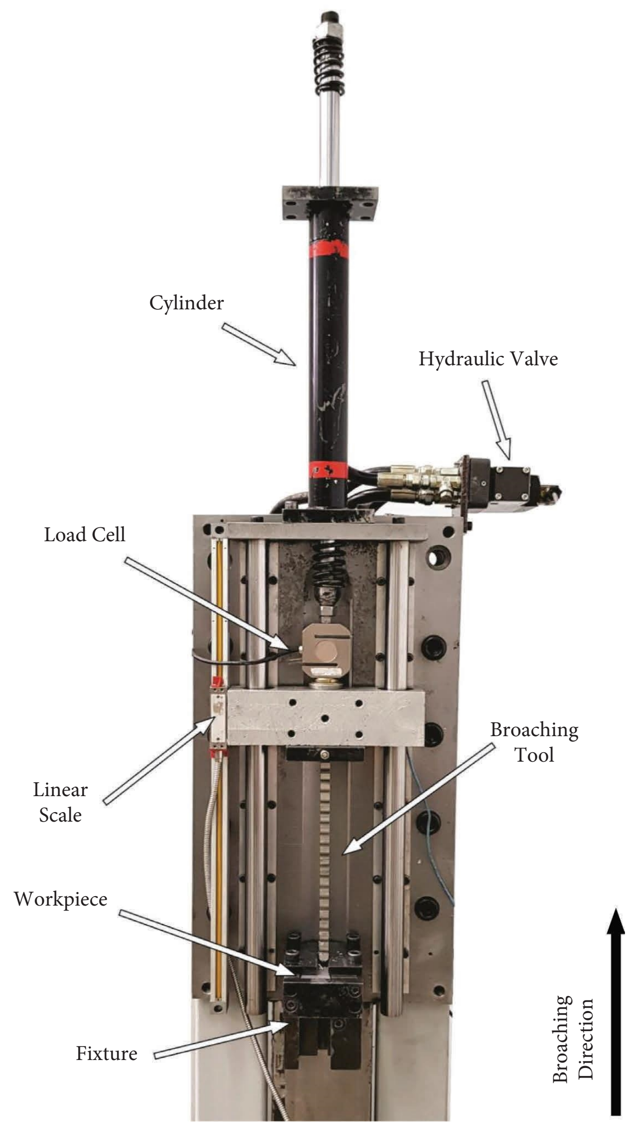

Figure 2: Servohydraulic system components [13].

In Figure 4, the broaching tool, as well as its dimensional characteristics extracted from the digitizer, can be seen. It consists of three main parts, the roughing teeth, where the rise per tooth is higher. They have the highest contribution to the material removal rate. Then, there are the finishing teeth, where the rise per tooth is lower, and they aim to improve the precision and surface roughness of the workpiece. Finally, the calibration teeth are responsible for ensuring the intended material is removed as expected.

Besides, there is a thorough hole at the end of the tool used for pulling the broaching tool through the guide in the broaching direction.

The workpiece material used for this study is phosphorbronze in the shape of blocks with dimensions of $30 \times 40 \times 40$ mm. The machined workpiece can be seen in Figure 5.

Each block is used for two different tests for material-saving issues. Besides, Table 4 shows the mechanical properties of the workpiece material.

The fixture of the setup is made of Mo40 alloy steel and is designed and manufactured in our lab.

The relief valve is used for setting, decreasing, or maintaining outlet pressure constant in fluid transfer lines.

Relief valves control the system pressure by bypassing pressured fluid from a secondary line. These valves are designed to act at a particular preset pressure and protect the pressured equipment and tank from overload. In the current study, considering other system demands and the hardware specifications implemented for the research, the relief valve preset pressure is set to 250 bars.

Besides the relief valve, the cylinder movement and speed are controlled by a servo solenoid hydraulic valve with electrical position feedback. The characteristics of hydraulic cylinders and valves are tabulated in Table 5.

The digital linear scale reads the position data with 5 μm precision. In addition, to carry out cutting force tests, the Dacell CX101-T30 high-precision load cell measures the cutting force in each test.

Before running the tests, the load cell was calibrated using different gauge blocks of already known weights. Taylor Hobson Surtronic 25 profilometer with the accuracy of 1 μm was implemented to measure the roughness parameter (R_z) of the broached workpiece. Table 6 illustrates the detailed specifications of the sensors implemented in the research.

The power unit includes an electric motor and pump, supplying oil with appropriate pressure and temperature for the servohydraulic valve. To stabilize the oil pressure, two accumulators are also installed in the pressure and return lines of the hydraulic circuit. The specifications of the motor and pump are listed in Table 7.

PID controller is one of the most common controllers used in industry and academic research. In the design of any controller, the aim is to create a logical balance between three characteristics: overshoot (M_p), settling time (t_s), and delay time (t_d). In PID controllers, this balance is reached through the value of three parameters: proportional (K_P), integral (K_I), and derivative (K_D).

The Ziegler–Nichols [23] heuristic method is implemented to acquire these parameters. At first, K_I and K_D are considered to be zero. Then, K_P is gradually increased until the system reaches a steady oscillating state. This value is

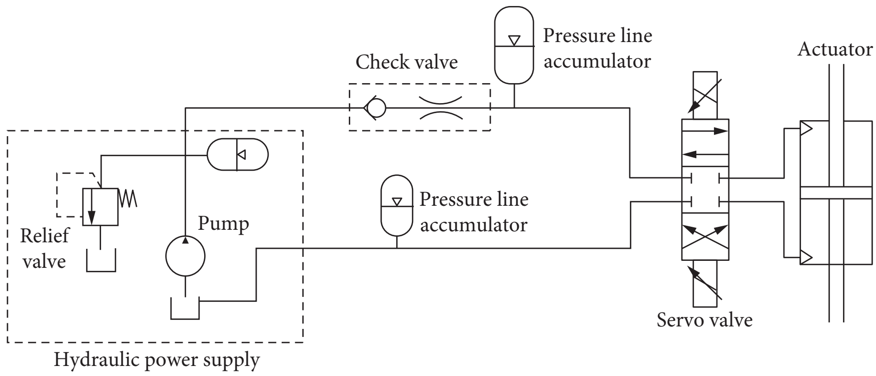

Figure 3: A simplified model of the hydraulic circuit [13].

Table 3: Specifications of the broaching tool.

Tool material	210Cr46 steel
Type	Pull end
Tooth width	13
Number of teeth	18
Rise per tooth	0.09 mm
Pitch	13.97 mm
Edge radius	5 μm
Rake angle	12.78°
Clearance angle	2.06°
Gullet radius	1.5 mm
Length of broach	200 mm
Cutting velocity	5–20 m/min

known as the ultimate coefficient (K_u), and the period of this steady oscillation is (T_u). Using K_u and T_u, K_P, K_I, and K_D are calculated. Having a rough yet educated estimation for PID parameters, experimental tests were carried out to narrow down these parameters to the optimum values presented in Table 8. Two PID controllers are required to provide operational freedom on the position and speed of the cylinder, the cutting velocity, and harmonic vibrations.

The first PID controller is designed to control the valve spool position and, accordingly, the position of the broaching tool. To determine the optimum K's for the "spool PID" shown in Figure 6, fifteen different experiments were conducted and carried out through which M_p, t_s, and t_d were simultaneously minimized. As shown in Figure 7, the PID block "Linear PID" is simulated in MATLAB 2019b and a SIMULINK circuit to enable speed control of the broaching process.

The optimum results of the experiments are given in Table 8. The second PID controller is designed to control the valve speed and enables us to add harmonic vibrations of the desired characteristics to the cutting velocity.

4. Procedure

Empirical tests for this research can be divided into two series. In the first series of experiments, phosphor-bronze block is broached (without vibration) at different cutting velocities of $V_C = 5$, 10, 15, and 20 m/min, then the cutting force and the workpiece surface roughness are measured and compared with the model.

In the second series of experiments, harmonic vibrations are applied to the cutting tool in the direction of the cutting velocity in the form of a sine wave with a constant amplitude of $A = 1$ m/min and frequencies of $F = 55$, 65, 85, and 95 Hz. To obtain interpretable results for the relationship between the cutting force, surface quality, and harmonic vibrations, the cutting velocity during every single test has to be constant. To ensure this along the cutting stroke, the desired speed must be obtained quickly (in this research, during the first 0.01 seconds of the process) by applying the maximum pressure of 200 bars. It has to be mentioned that higher frequencies were not chosen due to the limitations of the experimental setup; however, the results with the chosen frequencies were already promising. Test results were then analyzed to investigate the influence of cutting velocity and forced vibrations on the cutting force and surface quality.

5. Results and Discussion

5.1. Cutting Force and Cutting Velocity. The average force in the roughing section of the tool is considered the cutting force for each cutting velocity. The cutting force-time graph for $V_C = 10$ m/min is plotted in Figure 8, which can verify the analytical model.

The graph is divided into three segments. There are three peaks in segment 1, each representing the engagement of a new tooth with the workpiece. Nevertheless, they are not considered in force analysis since the process had reached the steady phase just after segment 1. In segment 2, there are five peaks, each of which stands for the initiation of engagement in the roughing section of the tool, preceded by segment 3, which contains three peaks resulting from three finishing teeth of the broaching tool. As the engagement of the tool workpiece initiates, the cutting force gradually increases until the maximum number of teeth is involved, i.e., three teeth.

Afterwards, the cutting force fluctuates in a specific range, reaching the end of the stroke, where the cutting force magnitude drops to zero after the last tooth leaves the workpiece. Figure 8 also shows the agreement between the experimental results and the simulated data.

The increase in cutting velocity has positive effects on the chip formation process and lowers the shearing coefficient of the workpiece, which consequently results in a lower cutting

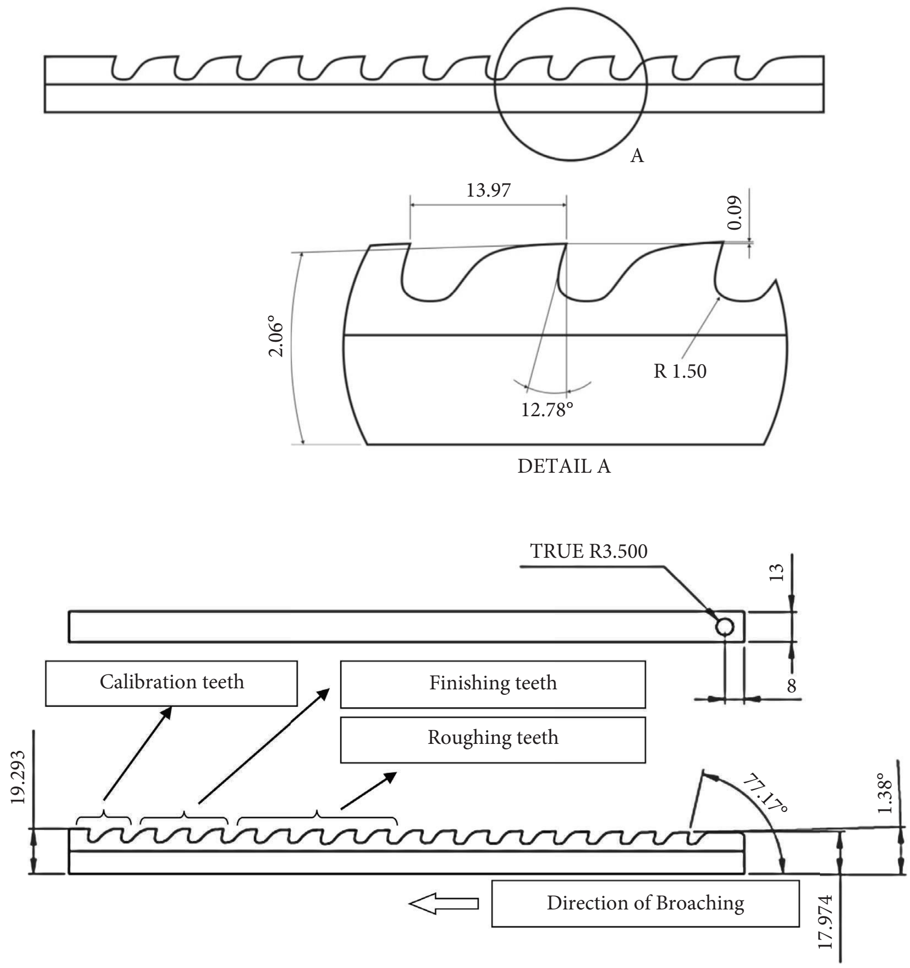

Figure 4: Extracted information from the digitizer for broaching tool.

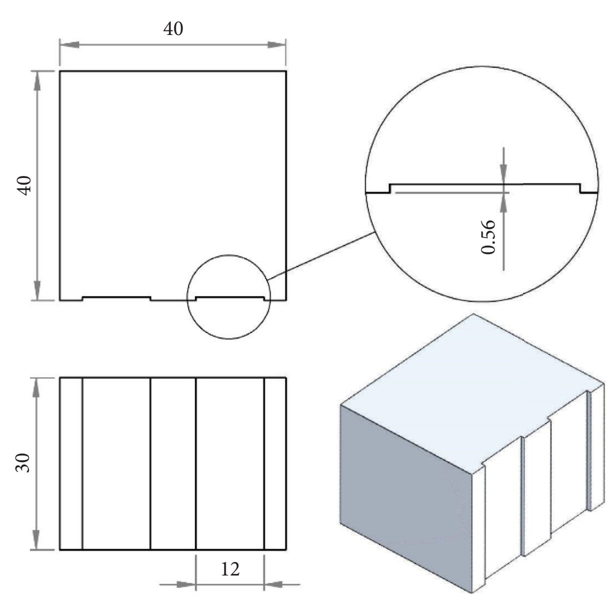

Figure 5: Broached workpiece.

Table 4: Mechanical properties of the workpiece material.

Material	Phosphor-bronze
Young's modulus (E)	110 GPa
Yield strength (σ_y)	531 MPa
Ultimate strength (σ_R) [21]	548 MPa
Strength coefficient (K)	0.51 GPa
Strain hardening exponent (n)	0.29
Chip compression ratio (ξ)	5
Shear strength (τ_y) [22]	0.65 σ_R
Average shear stress (τ_c)	497 MPa

force. A case in point is the increase in cutting velocity from $V_C = 5$ to 20 m/min, where the average cutting force encounters a decrease of at least 20% from 4600 to 3600 N, respectively. Figure 9 shows the comparison of cutting force at different cutting velocities.

Figure 10 shows the engagement and disengagement of the tool tooth with the workpiece. At the start of the engagement, three teeth are responsible for material removal, causing a peak in the force diagram, while with the disengagement of a tooth, the magnitude of the force falls dramatically. The rise and fall of the force are strongly dependent on "rise per tooth," which is obviously higher in the roughing section, causing higher peaks in that area.

The increase in the cutting force for each engagement of a new tooth at different cutting velocities varies depending on the value of the cutting velocity with an

Table 5: Valves and cylinder specifications.

Relief valve	Manufacturer	Diplomatic
	Technical code	MCD6-SP/51 N/K
	Pressure limit	Up to 350 bar
	Max flow	75 L/min
	Fluid temperature	−20 to 80°C
	Viscosity	25 cSt
Servo valve	Technical code	4WRPH 6 C3B12L
	Nominal flow	12 L/min
	Voltage	24 V/min
	Actuator	Servo solenoid
	Max working pressure	250 bar
	Max solenoid current	2.7 A
Hydraulic cylinder	Cylinder type	Two-way
	Cylinder diameter	40 mm
	Piston diameter	25 mm
	Displacement	195 mm
	Max pressure	210 bar

Table 6: Sensors specifications.

Linear scale	Precision	5 μm
	Max working speed	60 m/min
	Supply	5 V
Load cell	Model	UU
	Capacity	1 ton
	Output	2 mV/V
	Working temperature	−20 to 80°C
Profilometer	Accuracy	0.001
	Display	8 inches
	Filter	Digital gauss
	Parameters	R_z

inverse relationship. At the cutting velocity of $V_C = 5$ m/min, per engagement of a new tooth in the roughing section of the process, an increase of 1400 N in the cutting force was observed, where the amount was reduced to 1100 N and 500 N at cutting velocities of 10 and 20 m/min, respectively.

It can be seen that when the cutting velocity is 20 m/min, the increase in cutting force per new engagement is around 700 N, while this amount is almost twice as much at 10 m/min, reaching $F_C = 1300$ N per engagement.

5.2. Cutting Force and Harmonic Vibrations. The next phase is to add intentional sine waves of predetermined amplitude and frequency to the cutting velocity to lower the cutting force. The sine wave has an amplitude of $A = 1$ m/min and frequencies of $F = 55$, 65, 85, and 95 Hz.

The general pattern of force diagrams is to some extent similar in both HVB and conventional broaching.

Notwithstanding, the results of the experiments show the hammering effect of the tool teeth on the workpiece. The sinusoidal cutting movement considerably differentiates the broaching motion in the conventional process and HVB. The intermittent contact between the tool and the workpiece in the direction of cutting velocity results in fluctuations in the corresponding cutting force and consequently leads to a reduction in its magnitude. Harmonic vibrations of the

Table 7: Hydraulic power pack specifications.

Electric motor	Type	3-phase
	Nominal power	1.1 KW
	Nominal revolution	1395 rev/min
Hydraulic pump	Type	Gear pump
	Volume	2.7 cm^3/rev
	Nominal flow rate	3.7 L/min
	Max pressure	250 bar

Table 8: Optimum PID parameters.

Parameter	Position control	Velocity control
t_s	0.727	0.217
M_p	0	0
t_d	0.523	0.103
K_P	0.2	5
K_I	2	0
K_D	0.001	0.001

tool created kinetic energy improved the chip formation process and enhanced the material removal rate.

Figure 11 shows the force-time graph for $V_C = 10$ m/min and the harmonic vibrations of $F = 95$ Hz.

It can explicitly show that the analytical model can be verified with the experimental procedure. Adding harmonic vibrations, depending on the magnitude of the frequency, lowers the cutting force by almost 20% at different cutting velocities. For instance, the average cutting force in the roughing section at $V_C = 10$ m/min is 4236 N, whereas, in the presence of harmonic vibrations of 95 Hz, this value decreases to 3180 N. Figure 9 shows the comparison of the magnitude of the cutting force in different cutting conditions.

The increase in cutting velocity and frequency of harmonic vibrations decrease the cutting force. By increasing cutting velocity, the chip formation process is enhanced, and the shearing coefficient between the workpiece material and the broaching tool tends to decrease, leading to a stable broaching process, and accordingly, the cutting force decreases. Besides, an increase in the frequency of harmonic vibrations has similar effects and causes a favorable decrease in cutting force by creating intentional interruptions in the broaching process.

5.3. Surface Quality and Cutting Velocity. A comparison of surface quality measurements in different cutting conditions is shown in Figure 12. In the first phase of the research, which is conventional broaching, an increase in cutting velocity from 5 to 20 m/min enhances the surface quality by up to 40%, reducing Ra from 3.2 to 1.8 μm.

In the second phase, which is harmonically vibrated broaching, the increase in vibration frequency from $F = 0$ to 95 Hz leads to a 35% reduction in surface roughness, reducing R_a from 3.2 to 2 μm in the cutting velocity of $V_C = 5$ m/min.

In comparison to conventional broaching at 5 m/min, adding a 95 Hz sine wave and increasing cutting velocity to 20 m/min enhances surface quality by up to 80%.

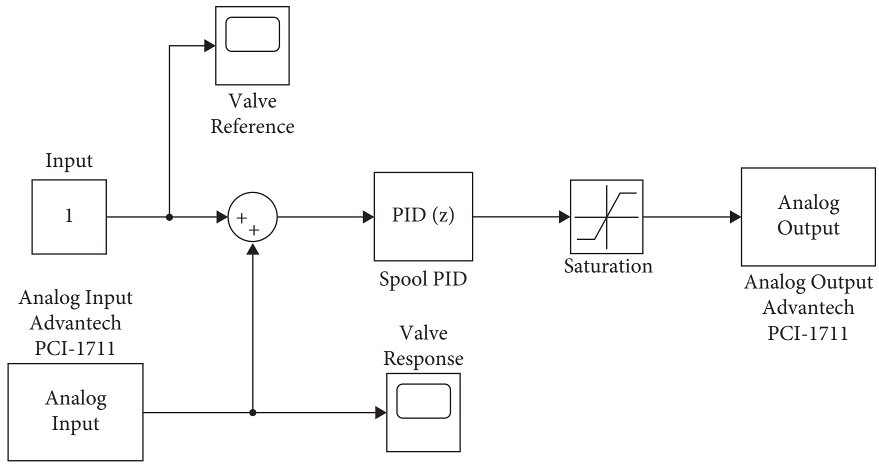

FIGURE 6: SIMULINK circuit for position control.

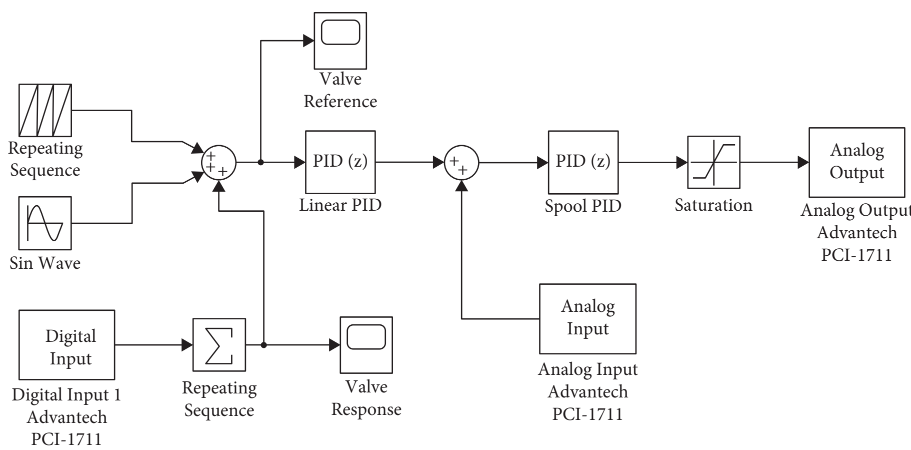

FIGURE 7: Position and speed control [13].

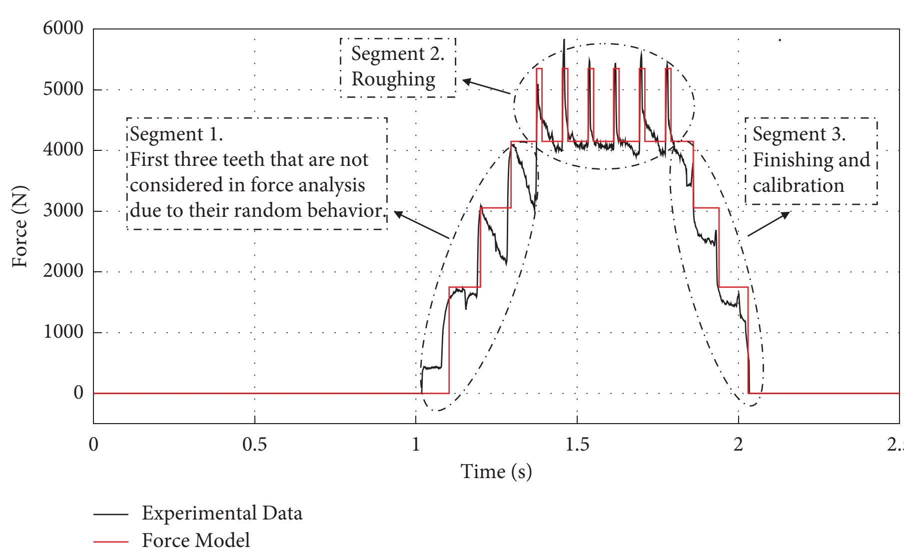

FIGURE 8: Cutting force vs. time graph for $V_C = 10$ m/min in conventional broaching acquired experimentally versus based on the simulated data.

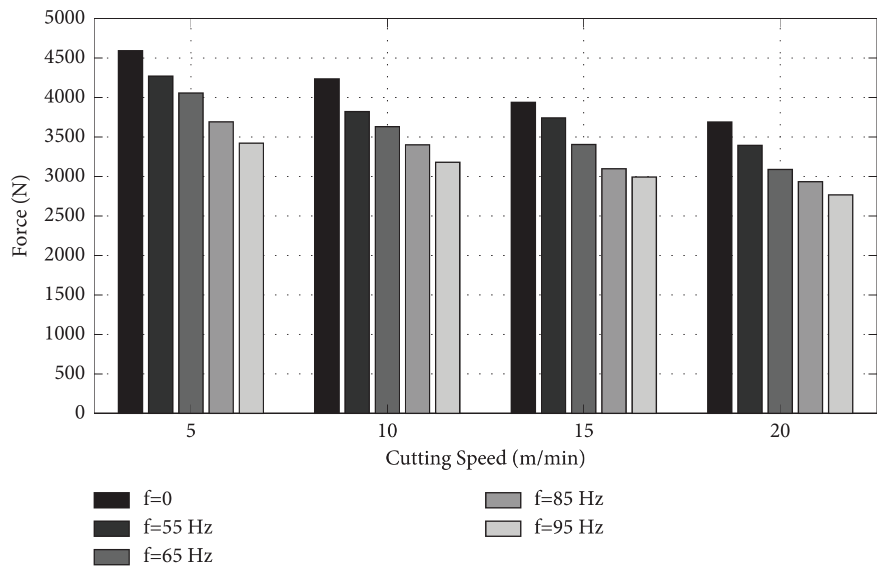

Figure 9: Comparison of the cutting force under different cutting conditions.

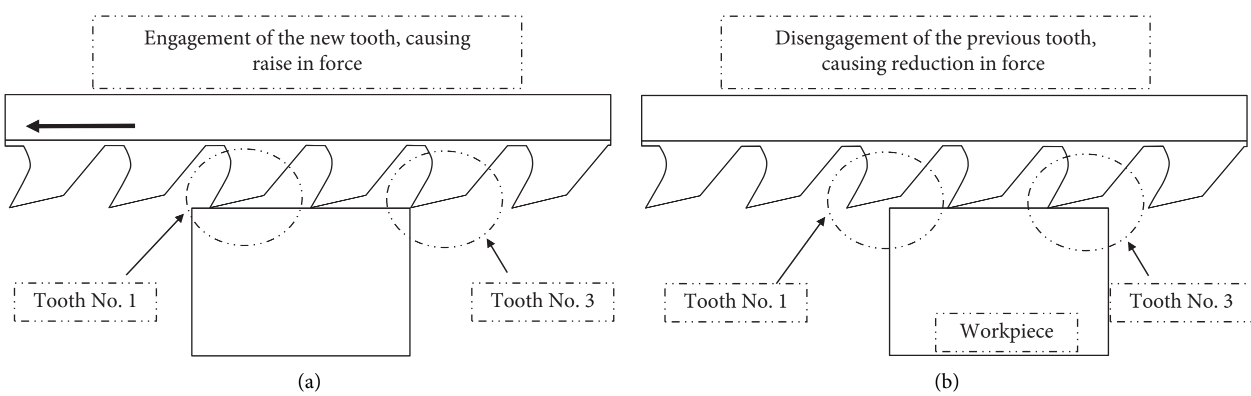

Figure 10: Engagement (a) and disengagement (b) of broaching tool teeth with the workpiece.

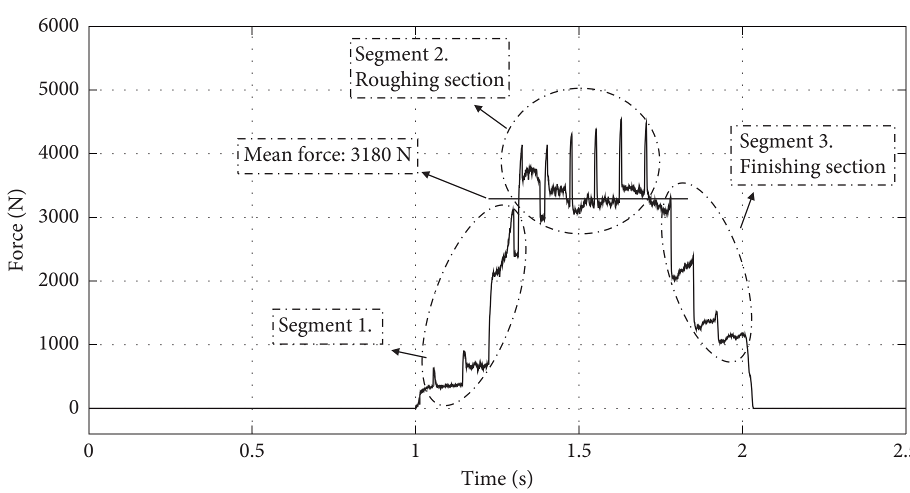

Figure 11: Cutting force vs. time graph for $V_C = 10$ m/min in harmonically vibrated broaching $F = 95$ Hz.

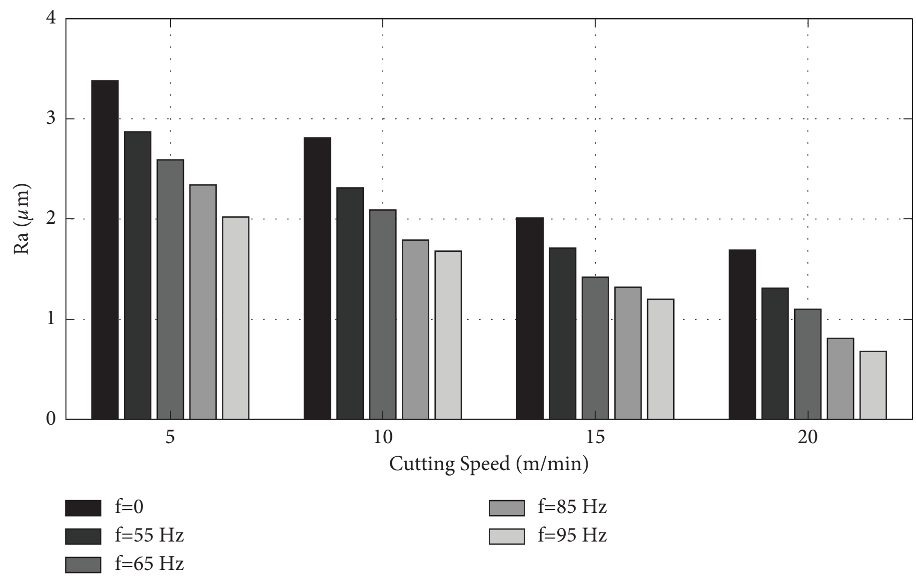

FIGURE 12: Comparison of surface roughness under different cutting conditions.

6. Conclusion

In this research, workpieces of phosphor-bronze material were broached under different cutting conditions.

(i) The experiments are significantly in agreement with the force model based on the components of the energy consumed in the broaching process.

(ii) The increase in cutting velocity from $V_C = 5$ m/min to 20 m/min causes a 40% reduction in surface roughness.

(iii) In addition to surface roughness enhancement, higher cutting velocity leads to lower cutting force, such that experiments revealed that the cutting force at $V_C = 20$ m/min is almost 20% lower in comparison to $V_C = 5$ m/min.

(iv) HVB at a higher vibration frequency leads to an elevated surface quality of 20% when a sine wave of $F = 95$ Hz is intentionally added to the broaching process compared to conventional broaching.

(v) Besides, HVB at $F = 95$ Hz, causes a 20% reduction in cutting force.

(vi) Per engagement of a tooth of the broaching tool, the cutting force magnitude increases sharply up to a peak, then falls gradually until a new engagement has occurred.

(vii) Based on the numerical approach and the experiments, for cutting velocities higher than 10 m/min, it is assumed that the cutting force will decrease, and the surface roughness will increase.

Nomenclature

A: Amplitude (m/min)
A_ω: Uncut chip cross-sectional area (m^2)
Br: Briks similarity criterion
b_{1T}: Chip width (m)
b_{fa}: Tool land (mm)
E_{fr}: Energy of fracture
F_C: Cutting force (N)
F_{fF}: The friction force between tool workpiece
F: Frequency (Hz)
f: Cutting feed per revolution (m/rev)
f_z: Depth of cut (m)
f_{cf}: Frequency of chip formation
K: Strength coefficient (N/m^2)
K_D, K_I, K_P: Derivative, integral and proportional coefficients
K_U: Ultimate coefficient
l_{ac}: Engaged length of cutting edge in the process (m)
l_c: Tool-chip contact length (m)
M_P: Overshoot
n: Hardening exponent of the workpiece material
P_C: Power consumed for cutting (N.m/min)
P_{fR}: Power (tool-chip interface) (N.m/min)
P_{fF}: Power (tool-workpiece interface) (N.m/min)
P_{pd}: Power consumed for plastic deformation (N.m/min)
P_{ch}: Power for formation of new surface (N.m/min)
$P_{mn\text{-}ce}$: Power consumed due to minor cutting edge (N.m/min)
R: Gullet radius (mm)
R_z: Mean roughness depth (μm)
t_{1T}: Uncut chip thickness (m)
t_{2T}: Formed chip thickness (m)
t: Pitch (mm)
t_d: Delay time (s)
t_s: Settling time (s)
T_U: Steady oscillations period
V_C: Cutting velocity (m/min)
V: Chip velocity (m/min)
α: Clearance angle (deg)

α_f: Tool orthogonal clearance (deg)
α_{nw}: Normal flank angle (deg)
γ: Rake angle (deg)
ρ_{ce}: Radius of cutting edge (m)
τ_y: Shear strength of workpiece material (N/m^2)
τ_c: Shear strength at the tool-chip contact zone
σ_R: Ultimate tensile strength of workpiece (N/m^2)
σ_y: Yield strength (N/m^2).

Data Availability

The authors declare that the data and the materials of this study are included within the article. The raw data are also available from the authors upon a reasonable request.

Ethical Approval

The authors confirm that this work does not contain any studies with human participants performed by any of the authors.

Consent

The author grants the publisher the sole and exclusive license of the full copyright in the contribution, which license the publisher hereby accepts.

Conflicts of Interest

The authors declare that they have no conflicts of interest.

Authors' Contributions

Mahdi Sadeqi Bajestani designed and performed the simulation work and experimental setup and Amirreza Mohammadian wrote the manuscript.

Acknowledgments

This project was financially supported by Ferdowsi University of Mashhad (research and technology grant ID: 3/40663).

References

[1] P. J. Arrazola, J. Rech, R. M'saoubi, and D. Axinte, "Broaching: cutting tools and machine tools for manufacturing high quality features in components," *CIRP Annals*, vol. 69, no. 2, pp. 554–577, 2020.
[2] H. Meier, K. Ninomiya, D. Dornfeld, and V. Schulze, "Hard broaching of case hardened SAE 5120," *Procedia CIRP, 14*, pp. 60–65, 2014.
[3] D. Kumar and H. Rajabi, "Effect of lubrication on a surface parameter of strip in cold rolling with oil in water emulsion," *International Journal of Applied Engineering Research*, vol. 14, pp. 3261–3267, 2019.
[4] D. Kumar, "A comparison between full-film and mixed-film lubrication of cold strip rolling," *International Journal of Applied Engineering Research*, vol. 14, pp. 3590–3597, 2019.
[5] E. Özlü, A. Ebrahimi Araghizad, and E. Budak, "Broaching tool design through force modelling and process simulation," *CIRP Annals*, vol. 69, no. 1, pp. 53–56, 2020.
[6] F. Klocke and A. Kuchle, "Manufacturing processes 1," *RWTHedition*, Springer, Berlin, Germany, 2011.
[7] A. del Olmo, L. N. López de Lacalle, G. Martínez de Pissón et al., "Tool wear monitoring of high-speed broaching process with carbide tools to reduce production errors," *Mechanical Systems and Signal Processing*, vol. 172, Article ID 109003, 2022.
[8] O. Forst, "Broaching manual," *BMS is an independently owned, American company*, vol. 3, 1932.
[9] W. R. Terry and K. W. Cutright, "Computer aided design of a broaching process," *Computers & Industrial Engineering*, vol. 11, no. 1-4, pp. 576–580, 1986.
[10] H. A. Kishawy, A. Hosseini, B. Moetakef-Imani, and V. P. Astakhov, "An energy based analysis of broaching operation: cutting forces and resultant surface integrity," *CIRP Annals*, vol. 61, no. 1, pp. 107–110, 2012.
[11] R. Teti, K. Jemielniak, G. O'Donnell, and D. Dornfeld, "Advanced monitoring of machining operations," *CIRP Annals*, vol. 59, no. 2, pp. 717–739, 2010.
[12] A. Hosseini and H. A. Kishawy, "Prediction of cutting forces in broaching operation," *Journal of Advanced Manufacturing Systems*, vol. 12, no. 1, pp. 1–14, 2013.
[13] D. A. Axinte, N. Gindy, K. Fox, and I. Unanue, "Process monitoring to assist the workpiece surface quality in machining," *International Journal of Machine Tools and Manufacture*, vol. 44, no. 10, pp. 1091–1108, 2004.
[14] E. C. Özelkan, Ö. Öztürk, and E. Budak, "Optimization of broaching design," in *Proceedings of the 2007 Industrial Engineering Research Conference*, p. 1232, Pittsburgh, PA, USA, May 2007.
[15] O. Ozturk and E. Budak, "Modeling of broaching process for improved tool design," in *Proceedings of the International Mechanical Engineering Congress and Exposition (IMECE)*, pp. 291–300, Washington, DC, USA, November 2003.
[16] D. A. Axinte and N. Gindy, "Tool condition monitoring in broaching," *Wear*, vol. 254, no. 3-4, pp. 370–382, 2003.
[17] Z. Meng, C. Wu, J. Ni, and Z. Wu, "Modeling and analysis of cutting force in vibration-assisted broaching (VAB)," *The International Journal of Advanced Manufacturing Technology*, vol. 91, no. 5-8, pp. 2151–2159, 2017.
[18] M. Orouji, M. S. Bajestani, and B. M. Imani, "The effect of cutting speed on cutting force and surface quality in roaching of aluminum," 2023, https://mme.modares.ac.ir/article-15-8436-en.pdf.
[19] M. S. Bajestani, B. Moetakef-Imani, and A. Hosseini, "Effects of harmonic vibrations of cutting speed on cutting force and surface quality in Al 7075-T6 broaching," *IFAC-PapersOnLine*, vol. 52, no. 10, pp. 276–281, 2019.
[20] V. P. Astakhov and X. Xiao, "A methodology for practical cutting force evaluation based on the energy spent in the cutting system," *Machining Science and Technology*, vol. 12, no. 3, pp. 325–347, 2008.
[21] R. N. Caron, "Copper alloys: alloy and temper designation," *Encyclopedia of Materials: Science and Technology*, vol. 9, pp. 1660–1662, 2001.
[22] G. Chryssolouris, *Manufacturing Systems: Theory and Practice*, Springer Science & Business Media, Berlin, Germany, 2013.
[23] K. J. Åström and T. Hägglund, "Revisiting the Ziegler–Nichols step response method for PID control," *Journal of Process Control*, vol. 14, no. 6, pp. 635–650, 2004.